Surface Review and Letters, Vol. 9, No. 1 (2002) 455–459
© World Scientific Publishing Company

GISAXS STUDY OF CADMIUM SULFIDE QUANTUM DOTS

P. DUBCEK and S. BERNSTORFF
Sincrotrone Trieste, SS 14 km 163.5, 34012 Basovizza (TS), Italy

U. V. DESNICA, I. D. DESNICA-FRANKOVIC and K. SALAMON
Ruder Boskovic Institute, Bijenicka 54, 10000 Zagreb, Croatia

In order to investigate the structure of semiconductor/glass composites prepared by ion implantation, the grazing incidence small angle X-ray scattering (GISAXS) technique was applied to CdS nanocrystals synthesized in SiO_2 by implanting separately the constituent Cd and S atoms with a dose of $10^{17}/cm^2$ each, which resulted in a Gaussian depth density distribution of the dopants. Subsequently the samples were annealed at 700°C in order to form CdS particles. Due to the high concentration of nanocrystalline CdS, the scattered intensity is not following simple homogenous film models. Instead, additional particle scattering contribution is detected, as well as a multiplicative contribution due to inplane (lateral) particle correlation. From the first one, the particle size is estimated to be 4.6 nm, while an interparticle distance of 15–25 nm is deduced from the latter. Taking into account the applied dose, these values suggest that either part of the Cd and S ions are still dissolved in the amorphous substrate after annealing, and thus are not contributing to the CdS nanoparticle formation, or that implanted atoms have diffused deeper into the substrate during annealing.

1. Introduction

Direct wide-band-gap II-VI semiconductors, including CdS, have a huge potential for a variety of applications, especially in the areas of light-emitting and light-detecting devices, photovoltaic conversion (solar cells), X-ray and γ-ray detection, etc. Systems of small dimensions (nanocrystals or quantum dots) exhibit considerably different optical and electronic properties than the bulk semiconductors due to quantum confinement. Due to the large optical nonlinearity as well as fast response times, systems of CdS crystallites buried in glass show promise for very interesting applications in optical devices such as waveguides, high-speed optical switches or bistable resonators.

The traditional method of preparing quantum dots in optical semiconductor devices is adding semiconductor components into glass melt. During the solidification process, however, one has not sufficient control over the growth process, which results in nonideal sample properties (defects, semiconductor surface states, fluctuations in dopant size and distribution). Most of these drawbacks are overcome by the novel technique of ion implantation.[1–3] In order to investigate the structure of films prepared by this new method, the grazing incidence small angle X-ray scattering (GISAXS) technique was applied to SiO_2 films, in which CdS nanocrystals had been synthesized by separate implantion of Cd and S, and which had been annealed subsequently.

2. Experimental

In this work, a SiO_2 substrate, about 1 mm thick, was implanted with a dose of $10^{17}/cm^2$ Cd and S atoms each. This resulted in a Gaussian depth density distribution of the dopants, with a peak volume concentration of about $6.3 \cdot 10^{21}$ cm^{-3} of each of the Cd and S atoms at $\sim$130 nm depth, as determined by Rutherford backscattering. This corresponds to 20% atomic fraction of Cd + S atoms (compared to host atoms), or $\sim$40% weight fraction. The sample was subsequently annealed at 700°C, to provoke diffusion and synthesis of CdS crystallites. In this way

a CdS-rich "film" was formed inside of the SiO_2 substrate.

The structure of the film was investigated by means of small angle X-ray scattering (SAXS). To avoid the problem of high absorption in the SiO_2 substrate, grazing incidence was applied (GISAXS).

For X-rays, the index of refraction of solids is less than 1, i.e. $n = 1\eta' - i\eta''$, where η' and η''? are the dispersion and absorption coefficient, respectively. Therefore, total reflection happens for angles smaller than $\alpha_C = (2\eta)^{1/2}$ (the critical angle). For larger angles, reflectivity decreases steeper than the value given by Fresnel theory due to deviations from ideal flatness. Together with the reflected beam a diffuse scattering is present. This diffuse scattering from a surface, measured under nonspecular condition, i.e. when the scattering angle is different from the incidence angle, yields information about structural features along the surface. With the change of incidence angle, the penetration depth is changing, and this can be used to probe different parts of the sample versus the distance from the top surface.

GISAXS measurements were performed at the ELETTRA synchrotron radiation source at Trieste (Italy), at the SAXS beamline, using an X-ray photon energy of 8 keV ($\lambda = 0.154$ nm). The shape and size of the incident beam was adjusted by slits ($h = 0.1$ mm, $w = 5$ mm). The sample was mounted on a stepper-motor-controlled tilting stage with a step resolution of 0.001°. The stage (and the sample surface) was aligned horizontally and parallel to the beam within 0.1°. Measurements were taken at different, fixed grazing angles on the sample, using a Gabriel type, gas-filled 1-D detector at a fixed position (this corresponds to the so-called detector scans taken with point detectors).

3. Results and Discussion

The diffuse scattering from a rough surface of a homogenous film is analyzed usually by distorted wave Born approximation (DWBA),[4] which gives the intensity of GISAXS from a rough surface as

$$I = \Delta n|T_\alpha|^2|T_\beta|^2 \exp\{-\mathrm{Re}(q_z^2)\sigma^2\}/|q_z|^2 \cdot \int \cos(q_x x)\{\exp[|q_z|^2 c(x)] - 1\}dx\,, \qquad (1)$$

where α and β are the grazing incidence and scattering angle respectively, the x direction is along the surface and within the scattering plane, while z is normal to the surface (see Fig. 1). Δn is the change in the refraction index, T is the Fresnel transmittance for a given angle, $\mathbf{q}$ is the scattering wavevector, σ is the surface roughness, $c(x)$ is the height–height correlation function, and Re stands for the real part of the complex number. In the case of a self-affine surface, whose deviation from average height (ideal flatness) follows normal distribution, the correlation function is given by (see e.g. Ref. 5)

$$c(x) = \sigma^2 \exp(-(x/\xi)^{2H})\,, \qquad (2)$$

where ξ is the inplane correlation length and H is the surface roughness exponent.

In the case of scattering from a thin film, due to the difference in electron densities between film and substrate, two additional contributions are present: scattering from the substrate surface and scattering due to height–height correlation between the film and the substrate surfaces. These are described in DWBA with expressions similar to Eq. (1). In our samples, there is a smooth transition between either side of the film and the surrounding substrate due to the Gaussian depth distribution of implanted ions. Therefore, due to a poor height–height correlation these contributions can be neglected.

However, when electron density fluctuations are present in the film, their contribution can be distinguished from the surface roughness contribution to the scattering.[6] Thus the common structure factor could be defined as a sum of the two components[7] $S(q) = S_R(q) + S_D(q)$, where $S_R(q)$ is the surface

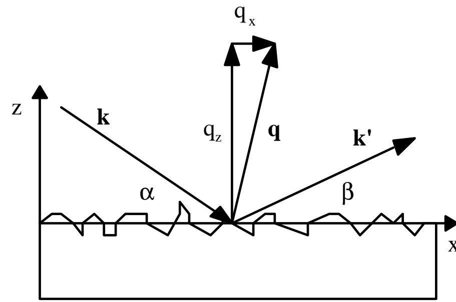

Fig. 1. Scattering from a rough surface. The roughness is a measure of deviation from the average surface (xy plane) in the z direction, while the height–height correlation is the correlation between two of those deviations.

roughness structure factor, and $S_D(q)$ is the electron density fluctuation contribution.

We believe that the structure factor sum is well applicable in the case of films with homogenous particle distribution in the film.

This is illustrated in Fig. 2, where GISAXS from an unimplanted substrate is compared to GISAXS from an implanted one. Note that between the Yoneda peak[8] and $2\theta = 3.5°$ the intensity for the unimplanted sample is increasing towards the specular peak, while it is decreasing for the implanted sample. When electron density fluctuations in the sample are present in the form of nanoparticles, their contribution to the structure factor should be added to the surface contribution, since the former should be independent of the grazing angle, apart from the absorption correction (which obviously is grazing-angle-oriented). Thus, since the substrate surface is not expected to be drastically deformed during the implantation (most of the energy transfer happens within the substrate while the implanted ions are being decelerated), the profound difference in the scattering intensity at very low angles is attributed to particle-like scattering added to the surface diffuse scattering. When a simple particle scattering model (Guinier approximation) is applied here, a Guinier radius of $R_G = 1.8$ nm is obtained, and this corresponds to a 4.6 nm sphere diameter [for spherical particles $R = (5/3)^{0.5}R_G$].

Another form of electron density fluctuation inclusion, namely the structure factors product $S(q) = S_R(q)S_D(q)$, has also been reported in the literature.[9] This is applicable in the part of the scattered intensity close to the specular peak (shoulders on either side of the peak). Since it is related to the specular angle, and in reference to Eq. (1), it is attributed to the inplane correlation function, namely the correlation of two particles offset in the z direction at a given particle-particle distance. Therefore, the surface roughness contribution from the scattering is deconvoluted numerically (here it was supposed that the total structure factor is a product of the roughness and density fluctuation constituents), and the obtained curves are plotted in Fig. 3. In this case the structure factor is obviously strongly determined by the inplane particle–particle correlation function. Although this kind of behavior has been reported[10] for monolayer island growth on the surface, in our case this explanation is not applicable because of the high energy used for the implantation. Also, in the case of flat islands, the correlation peak would be much better resolved. However, we expect that there is a high lateral (parallel to the substrate surface) ordering of the formed quantum dots, be it in size or in shape of the nanoparticles, since their concentration is very high.

The position of the shoulder (or lateral peak) is then interpreted — for a given grazing angle — as a measure of the mean interparticle distance within the same depth. This is plotted in Fig. 4 as a function of the penetration depth for a given grazing angle.

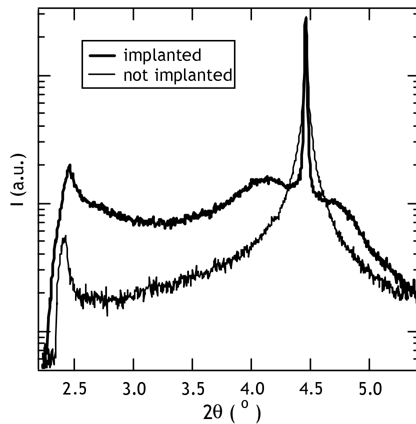

Fig. 2. GISAXS from implanted and nonimplanted SiO2 substrate for the same grazing angle (2.25°) vs. the total scattering angle normalized to the same specular peak intensity.

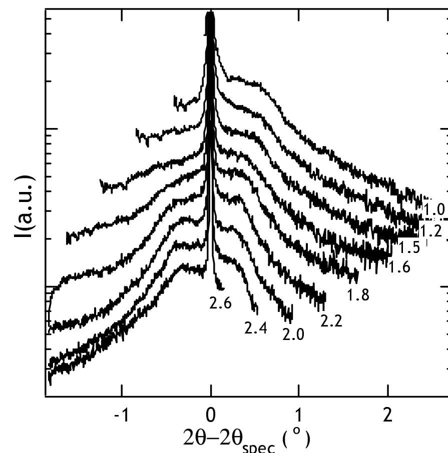

Fig. 3. Inplane correlation part of GISAXS from ion(Cd and S)-implanted SiO_2 vs. offset from specular angle, for diverse grazing incidence angles (in degrees, as indicated). The curves are offset vertically for clarity.

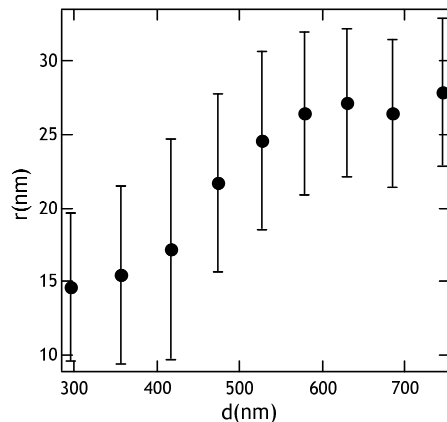

Fig. 4. Inplane correlation length (mean interparticle distance) vs. X-ray penetration depth.

Given the 20% atomic fraction of Cd + S, and the Guinier radius of 1.8 nm calculated from the low angle part of GISAXS, the interparticle distance should be about 7 nm, if all of the implanted Cd and S atoms were engaged in CdS nanoparticle formation. The values plotted in Fig. 4 suggest that either this is not the case, or that the layer containing CdS expanded during the annealing.

The penetration depth is gauged from the value of the critical angle, which gives the information about overall density, the irradiation dose, giving the partial Cd + S density, and expected implanted ion depth distribution. However, after annealing the Cd and S atoms are redistributed. This can be a source of major error, because the implantation parameters suggest that the particles are built-in mainly within a 250 nm depth from the substrate surface which could have changed during annealing.

The error in the interparticle distance value in Fig. 4 is a consequence of the correlation peak being poorly resolved. This lack of resolution is partly a consequence of a certain interparticle distance distribution, and indicates also that round particles, and not flat islands, are formed.

4. Conclusion

In contrast to the traditional methods of preparing quantum dots in optical semiconductor devices which are suffering from significant drawbacks, a newly proposed technique of separate ion implantation into solid substrates with subsequent annealing was used to prepare CdS quantum dots in amorphous SiO_2. The irradiation dose was $10^{17}/cm^2$ each and the annealing temperature was 700°C. In order to investigate the structure of the films prepared by this new method, the grazing incidence small angle X-ray scattering (GISAXS) technique was used. Due to the high concentration of nanocrystalline CdS, the scattered intensity is not following the simple models for homogenous film scattering.

Apart from the surface roughness scattering, two different contributions have been identified: (a) the particle scattering from within the film, giving an additive contribution to the scattering, and (b) the inplane particle correlation contribution as a multiplicative correction to the homogenous film surface scattering.

From the first one, the particle diameter is estimated to be about 4.6 nm, while the latter indicates the interparticle distance to be in the range of 15–25 nm. These values suggest that either not all of the implanted ions are taking part in CdS formation, or that CdS redistribution took place during the annealing.

The optical properties of quantum dots depend heavily on nanoparticle sizes and distribution. Thus, further studies are planned in order to better determine the influence of sample preparation parameters on nanoparticle formation.

Acknowledgments

This research was partly supported by the Ministry of Science and Technology of Croatia. The sample has been kindly provided by C. W. White from the Oak Ridge National Laboratory.

References

1. C. W. White, A. Meldrum, J. D. Budai, S. P. Withrow, E. Sonder, R. A. Zuhr, D. M. Hembree Jr., M. Wu and D. O. Henderson, *Nucl. Instrum. Methods Phys.* **148**, 991 (1999).
2. J. D. Budai, C. W. White, S. P. Withrow, M. F. Chisholm, J. Zhu and R. A. Zuhr, *Nature* **390**, 384 (1997).
3. A. Meldrum, L. A. Boatner and C. W. White, *Nucl. Instrum. Methods Phys.* **B178**, 7 (2001).
4. S. K. Sinha, E. B. Sirota and S. Garoff, *Phys. Rev.* **B38**, 2297 (1988).
5. S. K. Sinha, *Physica* **B173**, 25 (1991).
6. W. L. Wu, *J. Chem. Phys.* **98**, 1687 (1993).
7. S. Dietrich and A. Haase, *Phys. Rep.* **260**, 1 (1995).

8. Y. Yoneda, *Phys. Rev.* **131**, 2010 (1963).
9. R. Stommer, U. Englisch, U. Pietsch and V. Holy, *Physica* **B221**, 10 (1996).
10. H. A. van der Vegt, W. J. Huisman, P. B. Howes and E. Vlieg, *Surf. Sci.* **330**, 101 (1995).

Copyright © 2002 EBSCO Publishing